2962 *Biochemistry* **2010,** *49,* 2962–2972
DOI: 10.1021/bi902218p

BIOCHEMISTRY
including biophysical chemistry & molecular biology
Article

Characterization of Recombinant Lysyl Oxidase Propeptide[†]

Siddharth R. Vora,[‡] Ying Guo,[‡] Danielle N. Stephens,[‡] Erdjan Salih,[‡] Emile D. Vu,[‡] Kathrin H. Kirsch,[§] Gail E. Sonenshein,[§] and Philip C. Trackman*,[‡,§]

[‡]*Department of Periodontology and Oral Biology, Boston University Henry M. Goldman School of Dental Medicine, Boston, Massachusetts 02118, and* [§]*Department of Biochemistry, Boston University School of Medicine, Boston, Massachusetts 02118*

Received December 28, 2009; Revised Manuscript Received February 18, 2010

ABSTRACT: Lysyl oxidase enzyme activity is critical for the biosynthesis of mature and functional collagens and elastin. In addition, lysyl oxidase has tumor suppressor activity that has been shown to depend on the propeptide region (LOX-PP) derived from pro-lysyl oxidase (Pro-LOX) and not on lysyl oxidase enzyme activity. Pro-LOX is secreted as a 50 kDa proenzyme and then undergoes biosynthetic proteolytic processing to active ~30 kDa LOX enzyme and LOX-PP. The present study reports the efficient recombinant expression and purification of rat LOX-PP. Moreover, using enzymatic deglycosylation and DTT derivatization combined with mass spectrometry technologies, it is shown for the first time that rLOX-PP and naturally occurring LOX-PP contain both N- and O-linked carbohydrates. Structure predictions furthermore suggest that LOX-PP is a mostly disordered protein, which was experimentally confirmed in circular dichroism studies. Due to its high isoelectric point and its disordered structure, we propose that LOX-PP can associate with extracellular and intracellular binding partners to affect its known biological activities as a tumor suppressor and inhibitor of cell proliferation.

The biosynthesis of mature and functional collagen- and elastin-containing extracellular matrices requires posttranslational modifications including lysine-derived cross-links (*1*). Lysyl oxidase catalyzes the final enzymatic reaction required for subsequent cross-link formation. The LOX gene encodes a 50 kDa proenzyme (Pro-LOX),[1] which is secreted from cells and then cleaved by procollagen C-proteinases (PCPs) (*2*, *3*). This processing yields a ~30 kDa mature enzyme (LOX) and an ~18 kDa propeptide (LOX-PP) (*4*). In addition to *LOX*, four other mammalian lysyl oxidase like genes have been found and are termed lysyl oxidase-like 1−4 (*LOXL1*−*4*) (*5*−*9*). These proteins possess significant sequence identity in the C-terminal catalytic regions, but LOX-PP has little similarity with the propeptide region of LOXL1 and no similarity with the corresponding regions of LOXL2−LOXL4 (*10*, *11*).

Apart from its role in the extracellular matrix, the *LOX* gene was found to have tumor suppressor properties (*12*, *13*). Early studies assumed that LOX enzyme activity was important for this tumor suppressor property. Addressing this issue, Palamakumbura et al. mapped this "RAS-recession" activity of the LOX gene, to the LOX-PP domain and not the active enzyme, in RAS-transformed NIH3T3 cells (*14*). This finding prompted additional investigations into biological activities of LOX-PP. Ectopic expression of LOX-PP in *Her-2*/*neu* driven cancer cells was found to inhibit anchorage-independent growth and migration and growth of tumors in a xenograft model (*15*). Data indicated that LOX-PP inhibits the phosphatidylinositol 3-kinase/AKT and the ERK1/2 MAP kinase pathways and downstream NF-κB and cyclin D1 (*15*). Similar results were obtained using pancreatic and lung cancer cell lines with further identification of BCL-2 as a downstream target of LOX-PP (*16*). LOX-PP was also found to inhibit fibronectin-mediated signaling via FAK and p130cas and fibronectin-stimulated haptotaxis of breast cancer cells (*17*). Recently, we found that LOX-PP inhibits the growth of prostate cancer cell lines, and data indicate that one mechanism is via the inhibition of FGF-2 binding to cell surface receptors (*18*). LOX-PP has been shown to inhibit proliferation of primary rat aorta smooth muscle cells and TNF-α stimulated MMP-9 expression (*19*). LOX-PP was found to accumulate in the cell layer of differentiating phenotypically normal MC3T3-E1 osteoblast cell cultures (*20*). Recent findings indicate that LOX-PP inhibits FGF-2 stimulated proliferation of primary calvaria osteoblasts and thereby inhibits osteoblast development in vitro (*21*). *LOX*−/− mice exhibit perinatal death caused by aortic aneurysms, cardiovascular dysfunction, and diaphragmatic rupture and abnormal collagen and elastin structure (*22*, *23*). Pischon et al. have reported a skeletal phenotype in *LOX*−/− mice, some features of which may be due to the absence of LOX-PP (*24*).

LOX-PP is unusual in that it is a highly basic protein with the potential for posttranslational modifications that could account for its slow mobility on SDS−PAGE. N-Linked glycosylation of Pro-LOX in the LOX-PP region is known (*4*), but O-linked glycosylation of LOX has not been previously investigated. As noted, several studies have now demonstrated important biological activities of recombinant LOX-PP (rLOX-PP) expressed and purified from transfected T-Rex-293 cells. The present study was initiated with the goal of characterizing structural aspects of

[†]Supported by NIH NIDCR R01 DE14066, NIH NCI CA82742, and Department of Defense Idea Award W81XWH-08-1-0349.

*To whom correspondence should be addressed. Telephone: (617) 638-4076. Fax: (617) 638-5265. E-mail: trackman@bu.edu.

[1]Abbreviations: LOX-PP, lysyl oxidase propeptide; rLOX-PP, recombinant lysyl oxidase propeptide; Pro-LOX, pro-lysyl oxidase; PCP, procollagen C-proteinase; FBS, fetal bovine serum; NMWL, nominal molecular weight; LC, liquid chromatography; ESI, electrospray ionization; MS, mass spectrometry; DTT, dithiothreitol; TPCK, tosylphenylalanine chloromethyl ketone; CID, collision-induced dissociation; CD, circular dichroism; TFE, trifluoroethanol; TCA, trichloroacetic acid; TGF-β, transforming growth factor β; PGE_2, prostaglandin E_2; ID, inherently disordered.

 Published on Web 03/01/2010

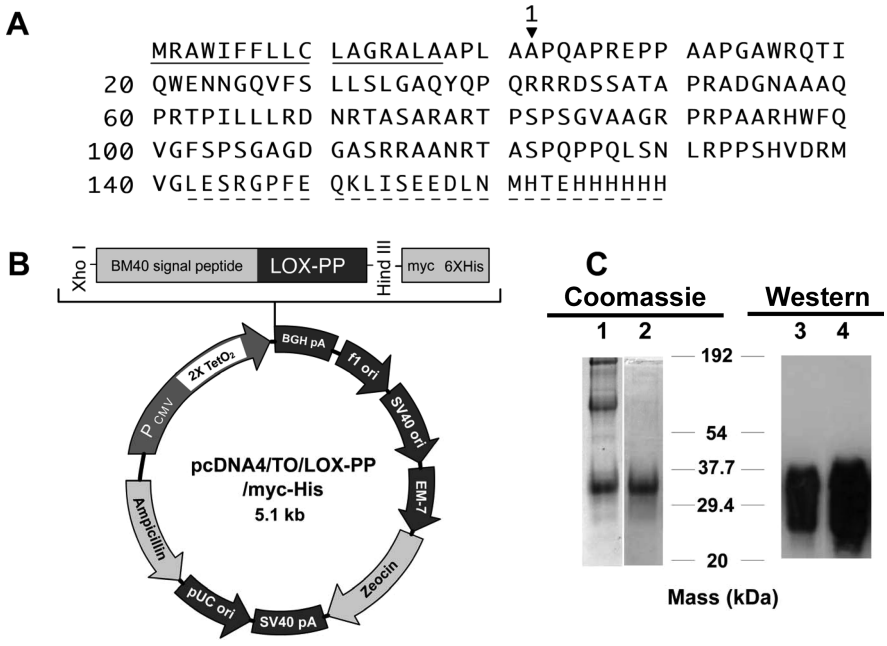

FIGURE 1: Expression and purification of rLOX-PP. Amino acid sequence of rLOX-PP (A), map of the pcDNA4/TO/LOX-PP/myc-His expression vector (B), and analysis of partially purified (lanes 1 and 3) and fully purified (lanes 2 and 4) rLOX-PP subjected to SDS−PAGE and stained with Coomassie G-250 based SimplyBlue SafeStain (lanes 1 and 2) or subjected to Western blotting using anti-LOX-PP antibody (*19*) (lanes 3 and 4).

rLOX-PP with an ultimate aim to gain new insights into possible structure/function relationships of LOX-PP.

MATERIALS AND METHODS

Expression and Purification of Recombinant LOX-PP. The T-Rex system (Invitrogen) was used to express recombinant rat LOX-PP (rLOX-PP) in mammalian cells. The LOX signal peptide (MRFAWTVLFLGQLQFCPLLRC) was replaced with the signal peptide of BM-40 (MRAWIFFLLCLABRALA). The pCEP-Pu/AC7 vector, containing the BM-40 signal peptide upstream of the C5 fragment of the collagen VI α3 sequence (kindly provided by Dr. Takako Sasaki, Max Planck Institute, Martinsried, Germany), was digested with *Nhe*I and *Xho*I and gel purified, thus removing the collagen sequence while retaining the BM-40 signal peptide sequence. In parallel, the rat LOX-PP sequence was first cloned from a rat LOX-PP construct in pcDNA3.1 with a forward primer designed containing an *Nhe*I site upstream of the LOX-PP sequence and a reverse primer containing a downstream *Xho*I site. The forward primer was 5′-ACTGCTAGCTGCCCCGCAG-3′, and the reverse primer was 5′-GTACCACCCGGAGCTCCAT-3′. The PCR products were then digested with *Nhe*I and *Xho*I and gel purified. The obtained LOX-PP fragment was ligated to the pCEP-Pu vector backbone, yielding the BM-40 signal peptide linked to the rat LOX-PP sequence. Next, this vector was digested using *Hin*dIII and *Xho*I yielding a fragment that contains a 5′UTR upstream of the BM-40 signal peptide−LOX-PP sequence. This fragment was finally inserted into the multiple cloning site of the pcDNA4/TO/myc-His-A vector (Invitrogen). The final construct was fully sequenced. The construct was designed to produce the rat LOX-PP sequence upstream of a c-myc and 6×His tag (Figure 1A) in an inducible expression system and is designated as pcDNA4/TO/LOX-PP/myc-His (Figure 1B).

The LOX-PP vector pcDNA4/TO/LOX-PP/myc-His (Figure 1B) was transfected into human embryonic kidney cells (T-Rex-293; Invitrogen), which stably express Tet repressor molecules from a pcDNA6/TR plasmid. Tet repressor molecules control the two tetracycline operator 2 (TetO2) sites present within the CMV promoter of pcDNA4/TO/LOX-PP/myc-His (Figure 1B), conferring tetracycline-inducible expression of the gene of interest (*25*). Stable T-Rex-293 cells expressing the pcDNA4/TO/LOX-PP/myc-His plasmid were selected in growth medium containing DMEM supplemented with 10% fetal bovine serum (FBS), 2 mM L-glutamine, zeocin (150 μg/mL), and blasticidin (5 μg/mL). Stable cells were induced for the production of LOX-PP by the addition of doxycyclin (1 μg/mL) in medium containing 2% FBS without zeocin. Cells were then cultured for 48 h, and LOX-PP was purified from the conditioned medium. Preliminary studies indicated that 48 h is the optimum time point for accumulation of LOX-PP in the conditioned medium (data not shown).

LOX-PP purification was accomplished by first filtering 250 mL of culture medium through a 0.45 μm filter followed by addition of sample dilution buffer (200 mM sodium phosphate buffer, pH 8.0) in a 1:1 ratio. This sample was applied to a nickel affinity column [Bio-Scale Mini Profinity IMAC cartridge (Bio-Rad)] preequilibrated with 100 mM sodium phosphate, pH 7.8, at a flow rate of 4 mL/min on an automated BioLogic DuoFlow chromatography system (Bio-Rad). The column was washed with equilibration buffer until the OD_{280} reached baseline levels, and the column was eluted with 8 M urea and 0.1 M sodium phosphate, pH 4.3. The eluate was found to have high molecular weight impurities (Figure 1C, lane 1). Hence, LOX-PP was further purified by ultrafiltration utilizing Amicon Ultra-15 centrifugal filter devices (Millipore) containing Ultracel membranes in series. First, a 50000 nominal molecular weight (NMWL) filter was used to separate the high molecular weight impurities in the retentate, while LOX-PP was recovered in the filtrate. This step was performed twice. The filtrates were then concentrated using a 10000 NMWL filter, where LOX-PP collected as the retentate, while lower molecular weight impurities were eliminated in the filtrate. The final retentate was dialyzed against three changes of

1 L each of ultrapure deionized water at 4 °C, using the Slide-A-Lyzer dialysis cassettes (10000 MWCO; Pierce). The concentrated, dialyzed, recombinant LOX-PP was stored at −80 °C. Aliquots were resolved by 12% SDS−PAGE and stained for protein using a Coomassie G-250 based SimplyBlue SafeStain (Invitrogen) to assess purity (Figure 1C, lane 2) and also subjected to Western blot analysis to ensure that the major band obtained is immunoreactive to anti-LOX-PP antibody (Figure 1C, lane 4). Typical concentrations obtained were ∼0.3−0.7 mg/mL [Advanced Protein Assay (Cytoskeleton)] and yields 0.5−1.0 mg of protein/L of culture medium.

MC3T3-E1 Conditioned Medium. Phenotypically normal murine preosteoblast MC3T3-E1 cells were treated with TGF-β1 essentially as described previously (*26*) to obtain conditioned medium that contains naturally produced LOX-PP detectable by Western blotting for comparison to rLOX-PP. MC3T3-E1 subclone 4 (ATCC) cells were maintained in α-MEM supplemented with 10% FBS, 1% nonessential amino acids, 100 units/mL penicillin, 100 μg/mL streptomycin, 50 μg/mL ascorbic acid, and 5 mM β-glycerophosphate at 37 °C and 5% CO_2 in a fully humidified incubator. When cells were 75% confluent, they were serum starved for 24 h followed by treatment with or without 400 pM TGF-β1 (Peprotech). After 18 h of treatment, culture media were collected, protease inhibitor cocktail (Sigma) was added, and then the mixture was centrifuged to eliminate cell debris. Supernatants were concentrated 10× using Amicon Ultra-15 centrifugal filter devices (Millipore) with 10000 NMWL filters.

Deglycosylation. Enzymatic deglycosylation assays were performed on recombinant LOX-PP and on MC3T3-E1 conditioned medium utilizing 20 μg of protein in a final volume of 10 μL as follows. To remove N-linked modifications, samples were treated with 5 units of PNGase F (Sigma) under native conditions in 100 mM sodium phosphate buffer, pH 7.5, for 4 h at 37 °C. To remove O-linked modifications, samples were first treated for 1 h with 1 milliunit of α(2−3,6,8) neuraminidase (Sialidase; Roche) to hydrolyze sialic acid residues, followed by the addition of 0.5 milliunit of *O*-glycosidase (Roche). In samples where all N- and O-linked glycosylations were to be removed, both classes of enzymes were used as indicated and incubated under native conditions in 100 mM sodium phosphate buffer, pH 7.5, for 4 h at 37 °C. At the end of the reactions, equal volumes of 2× sample buffer (62.5 mM Tris-HCl, 2% SDS, 0.71 M β-mercaptoethanol, and 10% glycerol) were added and boiled for 5 min. Samples were then resolved in a 12% SDS−PAGE gel and stained for protein using a Coomassie G-250 based SimplyBlue SafeStain (Invitrogen) or subjected to Western blotting as described below. Control reactions containing either rLOX-PP or MC3T3-E1 conditioned media proteins without deglycosylation enzymes were incubated in parallel, as negative controls.

SDS−PAGE and Western Blotting. Deglycosylated and control samples were resolved by electrophoresis using a 12% SDS−PAGE gel and transferred onto PVDF membranes, followed by Western blotting. Membranes were blocked for 2 h in 5% nonfat dry milk in TBST (20 mM Tris-HCl, pH 8.0, 150 mM NaCl, 0.5% Tween) and then incubated with anti-LOX-PP antibody (1:6000) (*19*) overnight in 5% milk−TBST. Membranes were washed three times each for 15 min in TBST followed by incubation with secondary antibody for 1.5 h. Membranes were washed, and the bound HRP-conjugated secondary antibody was detected using enhanced chemiluminescent reagent (ECL, Amersham).

Mass Spectrometry. Nondeglycosylated or deglycosylated rLOX-PP samples in 50 mM NH_4HCO_3, pH 8.0, were hydrolyzed with specific proteases to generate peptides for MS-based sequencing technologies at Boston University Henry M. Goldman School of Dental Medicine, Department of Periodontology and Oral Biology. TPCK-treated trypsin 2% (w/w) (Sigma-Aldrich) was added to rLOX-PP and incubated overnight at 37 °C. Alternatively, samples were digested using 2% (w/w) chymotrypsin and Asp-N sequentially. Where indicated, samples were treated with 10 mM dithiothreitol (DTT) or deuterium-labeled DTT ([D_6]DTT) in the presence of 0.25 M NaOH at 50 °C for 1 h to derivatize O-glycosylated serine and threonine residues. Samples were then neutralized using dilute HCl followed by the addition of trifluoroacetic acid to a final concentration of 0.1% (v/v). These samples were subjected to reverse-phase HPLC on a TSK-gel 5 μm, ODS-120T C18 (25 × 0.46 cm) column (TOSOHaas) to remove excess DTT reagent. Liquid chromatography−electrospray ionization−mass spectrometry (LC-ESI-MS/MS) analyses were carried out using an LTQ-linear ion trap mass spectrometer (Thermo Electron). Samples were suspended in 97.4% H_2O:2.5% CH_3CN:0.1% formic acid, and MS/MS analyses were carried out using an online autosampler (Micro AS; ThermoFinnigan) with autoinjections of 3 μL onto an in-line fused silica microcapillary column (75 μm × 10 cm), packed in-house with C18 resin (Micron Bioresource Inc.) at a flow rate of 250 nL/min. Peptides were separated by a 55 min elution comprising of multistep-linear gradient using a Surveyor MS Pump Plus (ThermoFinnigan). The eluted peptides were directly nanoelectrosprayed, and the MS/MS data were generated using a data-dependent acquisition with a MS survey scan range between m/z 390 and 2000. This data-dependent acquisition began with the LC separation which generated a total ion chromatogram in a survey scan followed by selection of specific ions for collision-induced dissociation (CID, MS/MS) in a descending order of signal intensity. All MS/MS spectra from LC-ESI-MS/MS were searched against the rat database, Uniprot (Universal Protein Resource, Version 9.0) as well as a custom database built using the known rat LOX-PP sequence with its expected tags from its parent vector. All searches were performed using the Bioworks 3.3.1 software and the SEQUEST search engine (*27*). The DTA generation was with precursor ion tolerance of 1.5 amu, fragment ion tolerance of 1.0 amu, and automated calculated charged states +1, +2, +3. The searches were performed with parameters for the specific enzymes used as well as no-enzyme specificity and modifications of serine and threonine residues by DTT (M_r +136.2) or deuterium-labeled DTT ([D_6]DTT) and run as a dynamic modification. The filtering criteria were as follows: Δcn > 0.1, probability < 0.1; for fully digested peptides, XCorr ≥1.6, 1.8, 2.5 for z = +1, +2, +3; for partially digested peptides, XCorr ≥1.8, 2.0, 3.0 and z = +1, +2, +3; and no enzyme, XCorr ≥2.0, 2.2, 3.5 for z = +1, +2, +3. In the analyses of the O-glycosylation modifications, a manual, static, tandem MS/MS was performed using the instrument method. The parent ion was subjected to MSn with increasing collision energy, each yielding a specific sugar moiety identified by the expected loss in m/z. The MS was performed "n" times until a LOX-PP peptide was identified. This peptide was then subjected to another round of tandem MS for sequencing.

Circular Dichroism (CD) Spectroscopy. Far-UV CD spectra were recorded using an Aviv circular dichroism spectropolarimeter (Model 215), equipped with thermoelectric temperature control. Four micromolar LOX-PP in 0.6 mL of 10 mM

sodium phosphate buffer (pH 7.2 or 4.8) or with 100 mM sodium chloride was placed in a 1 mm path-length quartz cuvette. Alternatively, 2,2,2-trifluoroethanol (TFE, $C_2H_3F_3O$; Sigma-Aldrich) was added to different final concentrations to 8 μM LOX-PP (10 mM sodium phosphate, pH 7.2) in a final volume of 0.3 mL in a 0.5 mm quartz cuvette. The spectra were recorded from 190 to 250 nm and averaged over three consecutive scans. Following buffer baseline subtraction, the spectra were normalized to LOX-PP concentration and are expressed as molar ellipticity ($[\theta] \times 10^{-3}$ deg cm^2 dmol^{-1}).

DNA Synthesis Assay. DNA synthesis was assayed by measuring [^{3}H]thymidine incorporation into MC3T3-E1 osteoblast cells as described previously (*21*). MC3T3-E1 cells were plated at a density of 2.5×10^4 cells/well in 24 well-plates and maintained in α-MEM supplemented with 10% fetal bovine serum (FBS), 1% nonessential amino acids, 100 units/mL penicillin, and 100 μg/mL streptomycin at 37 °C and 5% CO_2 in a fully humidified incubator. Twenty-four hours after plating, cells were transferred to serum-free medium containing 0.1% BSA for an additional 24 h. Cells were then treated with 1 ng/mL FGF-2 (Peprotech) or PBS with or without 4 μg/mL rLOX-PP for 24 h. Where indicated, rLOX-PP was preheated at 90 °C for 20 min and cooled before adding to cell cultures. For the last 6 h of induction, 2 μCi of [^{3}H]thymidine was added to each well. At the end of the incubation period, cells were washed three times in ice-cold PBS followed by two washes of 5% trichloroacetic acid (TCA) for 30 min each on ice. Wells were washed again in ice-cold PBS, and acid-insoluble precipitate was harvested in 0.2 N NaOH and 0.5% SDS and subjected to liquid scintillation counting (Packard Tri-Carb 1500).

RESULTS

Recombinant LOX-PP Expression. We previously expressed recombinant LOX-PP in *Escherichia coli* (*28*), which resulted in low yield of LOX-PP that precipitates in the absence of urea. Since LOX-PP is glycosylated by mammalian cells (*29*), a mammalian expression system was employed here with an aim to increase yield and solubility of rLOX-PP. Rat LOX-PP cDNA was used, encoding a protein that is 93% identical to the mouse and 72% identical to the human LOX-PP (Figure 1) . The rat LOX signal peptide (MRFAWTVLFLGQLQFCPLLRC) was replaced with the signal peptide of osteonectin, also known as BM-40 (MRAWIFFLLCLABRALA), based on its success in promoting synthesis and secretion of a wide variety of recombinant extracellular matrix proteins and enzymes (*30*). This cDNA was cloned into the tetracycline-inducible pcDNA4/TO/myc-His (Figure 1B) vector (*25*) in frame with the myc/His tag, and stable transfectants of human embryonic kidney cells (T-Rex-293) were obtained. LOX-PP production was induced and rLOX-PP protein purified to homogeneity from conditioned media as described in Materials and Methods (Figure 1C). rLOX-PP produced is recognized by the LOX-PP antibody, as expected (Figure 1C, lanes 3 and 4).

rLOX-PP Is N- and O-Glycosylated. Rat LOX-PP has a calculated molecular weight of M_r 15300. However, rLOX-PP produced in 293 cells migrates at ~33 kDa in reducing SDS−PAGE (Figure 1C). The propeptide domain of lysyl oxidase has two predicted N-glycosylation sites and several possible O-glycosylation sites, though Pro-LOX has not been previously shown to contain any O-linked carbohydrates. To investigate LOX-PP glycosylation, rLOX-PP was treated with

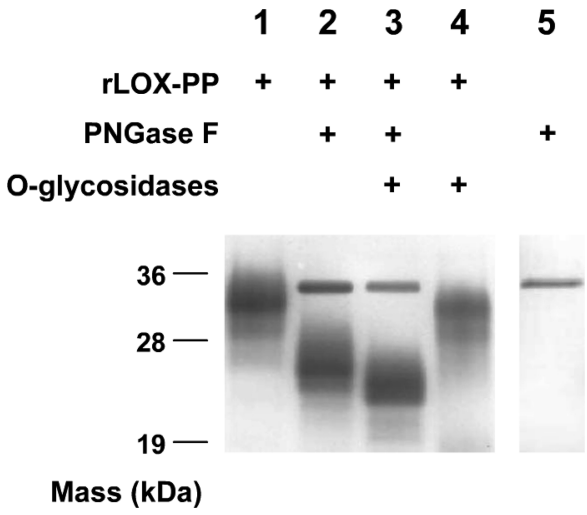

FIGURE 2: Recombinant LOX-PP contains both O- and N-linked sugars. Recombinant LOX-PP was treated with a combination of deglycosidases to remove N- and/or O-linked sugars followed by resolution on a reducing SDS−PAGE gel and stained with Coomassie G-250 based SimplyBlue SafeStain. Lane 1, rLOX-PP; lane 2, rLOX-PP + PNGase F; lane 3, rLOX-PP + PNGase F + *O*-glycosidases (neuraminidase and *O*-glycosidase); lane 4, rLOX-PP + *O*-glycosidases only (neuraminidase and *O*-glycosidase); lane 5, PNGase F alone. Molecular mass markers are indicated in kDa. All shifted bands are immunoreactive with the anti-LOX-PP antibody on a Western blot (Supporting Information Figure S1).

PNGaseF to remove N-linked sugars and a combination of α-neuraminidase (sialidase) and O-glycosidase to remove O-linked sugars (*31*). Deglycosylated rLOX-PP was then resolved on a SDS−PAGE. Enzymatic removal of N-linked carbohydrates substantially increased the mobility of LOX-PP (Figure 2, lanes 1 and 2). Removal of O-linked carbohydrates also increased LOX-PP mobility (Figure 2, lane 4) and suggests that LOX-PP contains O-linked carbohydrates. Upon combining both N- and O-glycosidases, rLOX-PP migrated still faster with a mobility corresponding to about M_r 22000 (Figure 2, lane 3), further indicating the presence of both N- and O-linked carbohydrates in the rLOX-PP.

We next wished to investigate whether naturally occurring LOX-PP is O-glycosylated. We treated MC3T3-E1 osteoblast cultures with TGF-β, which is known to enhance the expression of both Pro-LOX and its processing enzyme BMP-1 (*26*, *32*). Culture media were collected after 18 h, and media proteins were subjected to deglycosylation (see Materials and Methods). Figure 3 shows that TGF-β induced the level of secreted Pro-LOX (50 kDa band, Figure 3A, lane 2) and strongly increased the accumulated levels of extracellular processed LOX-PP (Figure 3B, lane 2). Treatment with O-deglycosidases caused the Pro-LOX and LOX-PP bands to each migrate slightly faster on SDS−PAGE (Figure 3A,B, lane 3). Treatment of media proteins with PNGaseF to remove N-linked sugars resulted in a dramatic increase in migration of Pro-Lox and LOX-PP (Figure 3A,B, lane 4). Importantly, a combination of both *N*- and *O*-deglycosidases resulted in increased migration to a sharp LOX-PP immunoreactive band with an apparent mobility corresponding to about M_r ~18000 (Figure 3B, lane 5). This indicates the presence of both types of modifications on naturally occurring LOX-PP. The faster migration of naturally occurring LOX-PP (Figure 3B) as compared to rLOX-PP (Figure 2) is likely due to the presence of the His/cMyc tag on rLOX-PP that has a predicted mass of M_r 3310. The difference in mobility on SDS−PAGE between

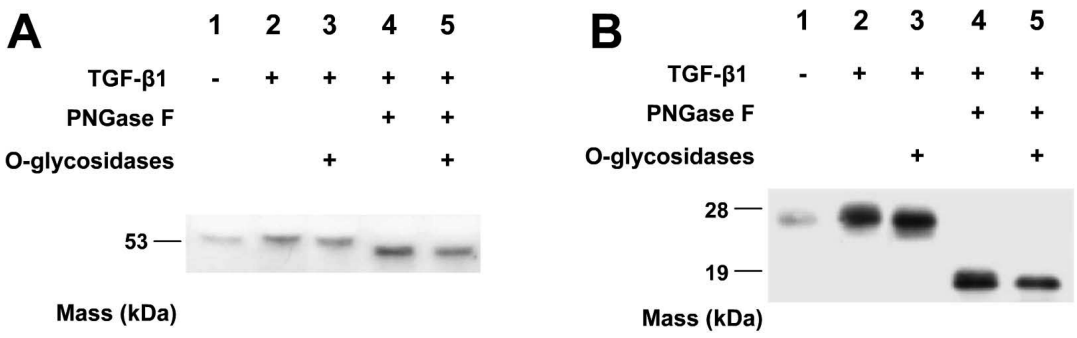

FIGURE 3: Natural LOX-PP contains both O- and N-linked sugars. Preconfluent MC3T3-E1 osteoblasts were treated with or without 400 pM TGF-β1 for 18 h. Media proteins were collected, concentrated, and deglycosylated (Materials and Methods). Deglycosylated samples were subjected to 12% SDS−PAGE gel followed by Western blotting with anti-LOX-PP antibody (*19*), resulting in bands corresponding to Pro-LOX (A) and LOX-PP (B). Lane 1, media proteins from no TGF-β1 controls; lanes 2−6, media proteins from cultures treated with TGF-β1; lane 2, TGF-β1-treated media proteins; lane 3, media proteins treated with *O*-glycosidases only (neuraminidase and *O*-glycosidase); lane 4, media proteins treated with PNGase F; lane 5, media proteins treated with both PNGase F and *O*-glycosidases.

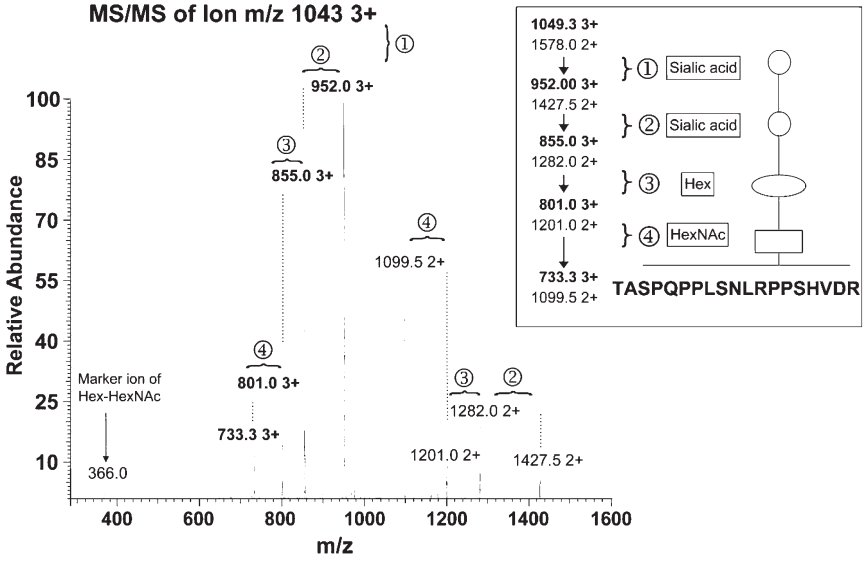

FIGURE 4: Tandem MS/MS to directly establish O-linked glycosylation of rLOX-PP. MS of a tryptic digest of rLOX-PP identified a unique ion 1049 3+ which, upon further ionization, resulted in a shift in the peak to 952.0 3+ corresponding to the loss of a sialic acid moiety [①]. Further ionization revealed shifts that are characteristic of the loss of another sialic acid [②], a hexose [③], and *N*-acetylhexosamine [④]. Final MS3 of the residual peak at 733 3+ (1099 2+) identified a peptide of rLOX-PP (TASPQPPQLSNLRPPSHVDR) (Supporting Information Figure S1) that contained the identified O-linked modification (inset).

naturally occurring LOX-PP and rLOX-PP is the apparent size difference of about M_r 3500, consistent with this notion. Both naturally occurring LOX-PP and rLOX-PP run slower on the SDS−PAGE than predicted as is typical for highly basic disordered proteins (see below).

Mass Spectrometry of rLOX-PP. rLOX-PP was analyzed by mass spectrometry (MS) to first confirm its amino acid sequence. A sample of the purified rLOX-PP was digested with trypsin and subjected to LC nanospray MS/MS. The MS/MS spectra obtained were searched against the rat rLOX-PP sequence as well as the rat protein database using the SEQUEST search engine. Peptides spanning ~66% of the total rLOX-PP sequence were identified. Peptide fragments containing heterogeneous modifications, such as glycosylations, cannot be recognized by this analysis, since their m/z ratios will not match expected parameters of known fragments. Therefore, initial scans of rLOX-PP contained multiple unidentified areas. Thus, samples obtained after both N- and O-deglycosylation were next subjected to proteolysis and LC/MS/MS, resulting in the identification of ~96% of the amino acids of rLOX-PP.

We next carried out MS analysis to directly investigate the presence of O-glycosylated rLOX-PP. A tryptic digest of rLOX-PP was subjected to an initial survey scan to obtain a total ion chromatogram as a function of time of elution from the C18 microcolumn. Unique parent ions were then individually subjected to collision-induced dissociation (CID) to look for shifts in peaks which are characteristic of fragmentation of carbohydrate moieties. An example is shown in Figure 4 for the unique ion with m/z 1049 with 3+ charged state, which was identified in the initial survey scan and subjected to further rounds of CID. This ion displayed a sequential loss of M_r 291, M_r 291, M_r 162, and M_r 203 for both the 3+ and the 2+ peaks upon respective sequential CID (Figure 4). These masses correspond to two sialic acids, one hexose (galactose/mannose), and one *N*-acetylhexosamine moiety, respectively. The residual peak after MS3 (m/z = 733.33, z = 3+, 1099, z = 2+) was identified as a peptide belonging to rLOX-PP (TASPQPPQLSNLRPPSHVDR) (Supporting Information Figure S2). These data provide direct evidence that rLOX-PP is O-glycosylated and identify the carbohydrate backbone structure of one O-linked posttranslational modification (Figure 4, inset).

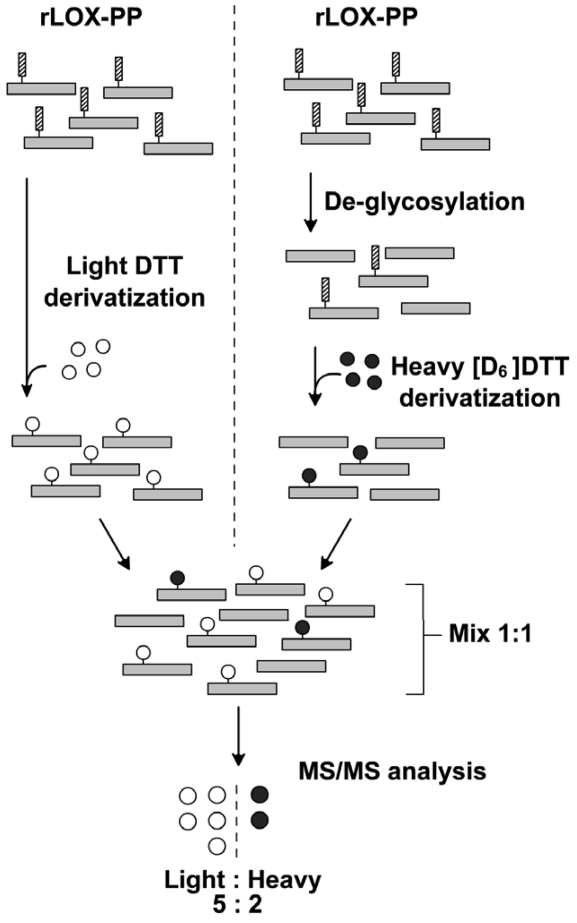

FIGURE 5: Experimental design for quantitative MS/MS analysis to identify sites of O-glycosylations on LOX-PP. Separate aliquots from the same preparation of rLOX-PP were either deglycosylated or not subjected to deglycosylation. Samples were then subjected to proteolysis with chymotrypsin and Asp-N. Nondeglycosylated samples were then derivatized with DTT (open circles) while deglycosylated samples were derivatized with heavy [D_6]DTT (filled circles). Equal amounts of nondeglycosylated and deglycosylated samples were mixed together and then subjected to LC/MS/MS. Three separate rLOX-PP preparations were subjected to this analysis. Software was instructed to recognize the same peptide fragment containing either the heavy or light DTT modification. Any Ser/Thr residue reactive with DTT but resistant to deglycosylation due to, for example, phosphorylation would have a ratio of 1:1 of heavy and light DTT, whereas glycosylated residues were declared if the ratio of light to heavy exceeded 1.5. Data from this analysis are presented in Table 1 and summarized in Figure 6.

The identified peptide contains one threonine and three serine residues, and our initial MS analysis did not reveal which of these amino acid residues is glycosylated, thus requiring further analyses. Unlike N-glycosylation, which occurs at the consensus motif Asn-X-Thr/Ser (X is any amino acid other than proline), several potential O-glycosylation motifs have been identified (*33*), and the modifications obtained are inherently heterogeneous in nature (*34*). Hence, not all sites that are predicted to be glycosylated will be utilized, and each site may be glycosylated to different extents (*35*, *36*). Prediction software NetOGlyc 3.1 (*37*), which produces neural network predictions to estimate the positions of potential O-linked glycosylation sites, was used to help identify possible sites of modification. The analysis suggested nine potential O-linked sites. Moreover, the peptide that we identified as being modified (Figure 4) contained three potential O-glycosylation sites predicted by NetOGlyc 3.1.c.

Table 1: Quantitative Analysis of MS/MS Peptides To Identify O-Glycosylation Sites in rLOX-PP[a]

sequence	LOX-PP (residue)	ratio (±CI) [O-deglycosylated (heavy): nondeglycosylated (light)]
Q.T*IQWENNGQVF.S	18	1:30.50 (±6.07)
A.AAQPRT*PILLLR.D	62	1:2.77 (±0.36)
N.LRPPS*HVDR.M	134	1:2.30 (±0.23)
R.MVGLES*RGPFEQK.L	tag	1:4.02 (±0.79)
K.LIS*EEDLNMH.T	tag	1:1.07 (±0.11)

[a]Equivalent amounts of nondeglycosylated and enzymatically deglycosylated samples of rLOX-PP were respectively derivatized with heavy/light DTT and analyzed by MS/MS as outlined in Figure 5; (*) DTT-modified residue. LOX-PP (residue) refers to position in the LOX-PP sequence as defined in Figure 6. Data are from experiments performed with three independent preparations of LOX-PP. The confidence interval for mean ratios is calculated for each peptide at a 5% level of significance. Ratios > 1:2 were considered to reflect significant differences in DTT modification as a function of enzymatic removal of O-linked carbohydrates.

Identification of Sites Modified by O-Linked Sugars. To directly identify O-linked glycosylation sites in rLOX-PP, quantitative MS analysis was performed. rLOX-PP was digested using chymotrypsin or Asp-N and subjected to β-elimination followed by DTT derivatization, which replaces the O-linked sugars with DTT (Materials and Methods). Phosphorylated Ser/Thr residues are also susceptible to DTT derivatization; hence to distinguish them from glycosylations, deglycosylated rLOX-PP were derivatized in parallel with native samples using deuterium-labeled DTT ([D_6]DTT). Equal amounts of the derivatized native and deglycosylated samples were then mixed together, and the abundance of residues containing (light) DTT and (heavy) [D_6]DTT in the mixture was analyzed by MS. A scheme illustrating the experimental design is provided in Figure 5. Three independent preparations of LOX-PP were each analyzed. Data identified three LOX-PP residues and one residue in the tag which were labeled more abundantly with light DTT as compared to heavy [D_6]DTT and are hence determined to be O-glycosylated (Table 1). For each of these residues, DTT derivatization is at least 2-fold greater under native conditions as compared to derivatization of the same residues postdeglycosylation. Moreover, one of the residues identified as being glycosylated (Ser 134) is present in the peptide identified by sequential CID shown in Figure 4 (TASPQPPQLSNLRPPS*HVDR). Taken together, these findings identify both a serine residue modified and the structure of the carbohydrate backbone carried on this particular serine residue. The use of the DTT-based technique is validated by the identification of an additional serine residue in the tag (K.LIS*EEDLNMH.T) that is equally labeled with heavy and light DTT (Table 1), indicating that DTT labeling of this residue is not affected by enzymatic deglycosylation and is therefore most likely phosphorylated (*31*, *38*). Moreover, this finding serves as an internal control and further validates analyses presented for LOX-PP O-glycosylation. A summary of glycosylation sites determined in rLOX-PP is provided in Figure 6.

Structural Analysis of rLOX-PP. The amino acid composition of LOX-PP (Figure 7A) is consistent with proteins that are inherently disordered (ID) (*39*). Specifically, LOX-PP has few large hydrophobic (Ile, Leu, Val) and aromatic residues (Trp, Tyr, Phe) with no Cys and few Asn residues. Conversely, it has a higher proportion of polar residues (Arg, Gln, Ser, Glu) and residues that help to create kinks in protein structure, such as Gly and Pro. Together, these "disorder-promoting" residues

```
                                    1
                                    ▼
    MRAWIFFLLC LAGRALAAPL AAPQAPREPP AAPGAWRQTI
 20 QWENNGQVFS LLSLGAQYQP QRRRDSSATA PRADGNAAAQ
 60 PRTPILLLRD NRTASARART PSPSGVAAGR PRPAARHWFQ
100 VGFSPSGAGD GASRRAANRT ASPQPPQLSN LRPPSHVDRM
140 VGLESRGPFE QKLISEEDLN MHTEHHHHHH
```

FIGURE 6: Glycosylated amino acid residues in LOX-PP. Residues are highlighted in black that were identified as containing O-linked sugars by MS analysis (data presented in Table 1). Serine 134 (*) of LOX-PP contains the identified O-linked modification: Ser-(HexNAc-Hex-sialic acid-sialic acid) (Figure 4). Consensus sequences for N-linked glycosylation of specific asparagine residues are underlined.

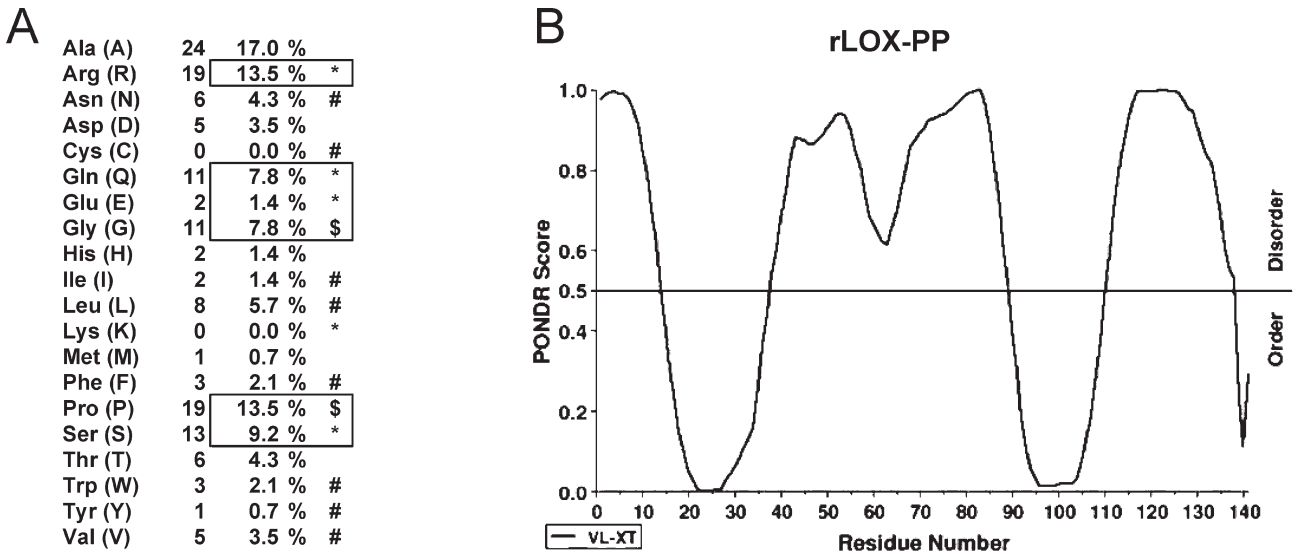

FIGURE 7: LOX-PP has a predominantly disordered structure. (A) Amino acid composition of rLOX-PP shows predominance of disorder-promoting residues (highlighted in box), including polar residues Arg, Gln, Ser, Glu "*" and structure-breaking residues Gly and Pro "$", and is scarce in order-promoting residues "#". (B) Prediction of order/disorder in rLOX-PP using PONDR. Based on the attributes of amino acids surrounding a residue, each residue (depicted on the *x*-axis) is assigned a disorder score (depicted on the *y*-axis) by the predictor. Predicted scores for residues ≥0.5 signify disorder. Analysis of LOX-PP returns a score of 67% disorder.

span the majority of the sequence of LOX-PP, accounting for about 70% of the overall amino acid composition (Figure 7A). Computer programs that predict potential ID regions/proteins based on the primary structure have been developed. The PONDR program (Predictor of Naturally Disordered Regions) generates a score between 0 and 1 based on amino acid residue attributes of charge, low aromatic content, fractional composition of particular amino acids, hydropathy, and sequence relationships (*39*, *40*). Scores between 0 and 0.5 indicate the presence of an ordered secondary structure while scores between 0.5 and 1.0 indicate the absence of an ordered secondary structure. PONDR analysis revealed that 67% of the LOX-PP sequence has scores greater that 0.5 (Figure 7B), suggesting that LOX-PP is largely disordered. Specifically, PONDR predicts disordered regions at the N- and C-terminal of LOX-PP and a central disordered region flanked by two ordered regions (residues 14−38 and 90−109).

To directly determine the degree of secondary structure in rLOX-PP, far-UV CD spectra were recorded. The spectrum of rLOX-PP in 10 mM sodium phosphate buffer at pH 7.4 at 25 °C (Figure 8A, ◆) demonstrated a negative peak centered near 200 nm, indicating a largely disordered structure (*41*). CD spectra were obtained in buffers with high ionic strength (10 mM sodium phosphate, 100 mM sodium chloride, Figure 8A, □), and in buffers with lower pH (10 mM sodium phosphate at pH 4.8, data not shown); all solvent ionic conditions yielded similar spectra, typical of disordered proteins. CD spectra were then obtained in the presence of increasing concentrations of TFE, an inducer of α-helical structure (Figure 8B). At concentrations ≥40% TFE, gradual spectral changes were observed, leading to formation of negative CD peaks at 222 and 208 nm and a large positive peak centered at 193 nm, which is characteristic of α-helical structure (*41*). These data indicate that LOX-PP can potentially acquire helical structure, a property that could be important for its function, with the potential to enhance its binding to biologically important partners.

rLOX-PP Is Biologically Active and Thermally Stable. Previous studies have reported that the LOX enzyme maintains activity when heated up to 65 °C and is further stable at 85 °C, although with reduced activity (*42*, *43*). To test whether LOX-PP is thermally stable, we used the previously established [^{3}H]thymidine incorporation assay as a measure of the biological activity of rLOX-PP (*21*). Figure 9 shows that rLOX-PP inhibits FGF-2-induced DNA synthesis in MC3T3-E1 osteoblasts to around 50%, in line with previously reported effects (*21*). Furthermore, LOX-PP is equally effective in inhibiting FGF-2-induced DNA synthesis when preheated to 90 °C. Additionally, heating of rLOX-PP to 90 °C did not result in precipitation and did not change the CD spectra (data not shown), indicating that, like the mature enzyme, LOX-PP is thermally stable.

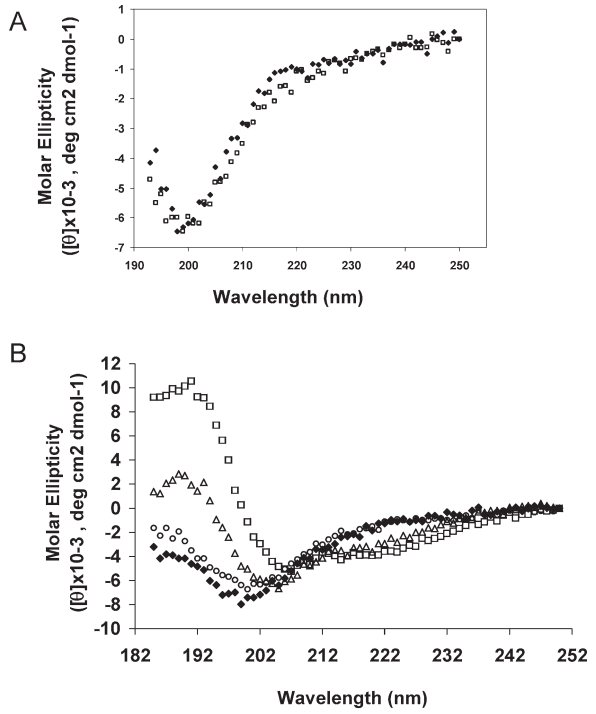

FIGURE 8: CD analysis of rLOX-PP. (A) Far-UV CD spectra (250−193 nm) of 8 μM LOX-PP acquired in 10 mM sodium phosphate buffer, pH 7.2 (◆), or 10 mM sodium phosphate buffer, pH 7.2, and 100 mM sodium chloride (◇). (B) Far-UV CD spectra (250−185 nm) of 4 μM LOX-PP acquired in 10 mM sodium phosphate buffer, pH 7.2, with increasing concentrations of TFE: 0% (◆), 20% (○), 40% (△), and 80% (□). Each spectrum is an average of three individual scans at 25 °C. For each condition, the baseline spectrum was recorded and subtracted from the spectrum of the protein. The *y*-axis depicts molar ellipticity ($[\theta] \times 10^{-3}$ deg cm^2 dmol^{-1}) plotted against wavelength on the *x*-axis.

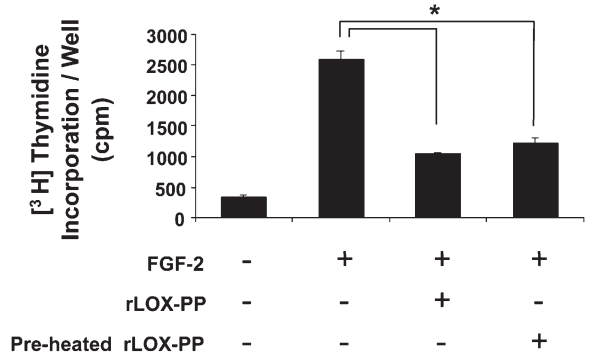

FIGURE 9: rLOX-PP is biologically active and thermally stable. MC3T3-E1 osteoblasts were grown in 24-well plates until 80% confluent and then placed in 0.1% BSA medium for 24 h. Cells were then treated with 1 ng/mL FGF-2 for 24 h in the presence of 4 μg/mL rLOX-PP that was either unheated or preheated to 90 °C. Incorporation of [^{3}H]thymidine into DNA was measured by TCA precipitation as described in Materials and Methods. Data shown are mean cpm values per well ± SD ($n = 3$; *, $p < 0.05$).

DISCUSSION

We report the production and characterization of biologically active rLOX-PP utilizing a mammalian system that yielded glycosylated, soluble rLOX-PP with more than 95% purity in good yield and show for the first time that rLOX-PP is both N-glycosylated and O-glycosylated. Rat and mouse Pro-LOX have two predicted N-glycosylation sites while human Pro-LOX has three, and all potential N-linked glycosylation sites are present in the propeptide domain (*4*, *44*). Naturally occurring Pro-LOX and LOX-PP made by murine MC3T3-E1 osteoblasts are similarly shown to contain both N- and O-linked carbohydrates. In light of the present report it may be of interest to investigate whether mature LOX contains O-linked carbohydrates.

DTT derivatization is used not only for identification of peptides containing O-linked carbohydrates but also for identification of phosphorylated serine and threonine residues (*45*). The isotopic labeling approach utilized here distinguishes phosphorylated residues from glycosylated residues by comparing the relative DTT derivatization of peptides derived from previously deglycosylated samples compared to native samples. The ratio of each DTT-derivatized peptide in the glycosylated compared to deglycosylated samples permits identification of glycosylated amino acid residues as we have reported here. Data indicate the presence of four O-glycosylated residues, all of which showed more than 2 fold decreased abundance of DTT modification after deglycosylation, as compared to native samples. A ratio close to 1 would imply the presence of a glycosidase-resistant DTT-reactive modification, most likely phosphorylation. One such residue was identified in the tag region of rLOX-PP, which may not be functionally relevant, but does serve as an internal control for the use of this technique in the identification of O-glycosylated residues.

Functions for carbohydrate structures in glycoproteins have been identified, ranging from influencing cell growth, cell−cell adhesion, protein turnover, and immune responses, serving as recognition markers and mediating interactions with pathogens (*46*, *47*). Our initial studies with nonglycosylated rLOX-PP produced in bacteria indicate that it is functional in inhibiting cell proliferation of osteoblasts and RAS-transformed fibroblasts, and it inhibits in vitro kinase activity of MEK2, a signal mediator in the RAS-ERK MAP kinase pathway (*14*, *19*, *28*). Carbohydrate chains are hydrophilic and can improve the thermal and kinetic stability of a protein (*48*), may protect against proteolytic degradation (*49*), or prevent precipitation and self-aggregation and improve solubility (*49*). In our experience, nonglycosylated LOX-PP expressed in *E. coli* (*28*) readily precipitates in the absence of urea. As there are no cysteine residues in rat LOX-PP, the solubility differences are most likely due to the presence of hydrophilic carbohydrate structures in rLOX-PP produced in T-Rex-293 cells.

Investigators have reported effects of mature LOX enzyme by using expression constructs of LOX. Some of these constructs are truncated, lacking the propeptide sequence. A report by Seve et al. (*50*) indicates that the complete elimination of the LOX-PP domain in expression constructs results in a loss of extracellular secretion of LOX enzyme, a finding confirmed by Min et al. (*15*). An earlier study (*51*) expressed a truncated LOX construct which retained some residues of the pro domain and resulted in active, secreted mature LOX enzyme. Taken together, these data identify the C-terminal residues 112−136 to be important in secretion of Pro-LOX. Interestingly, this region contains one of the two N-glycosylation sites and Ser 134 that we show here to be O-glycosylated in rLOX-PP. Carbohydrate moieties often act as "tags" to sort proteins into their correct subcellular compartments (*52*), and the absence of these glycosylations can result in the protein being withheld in the endoplasmic reticulum by the "quality control" machinery (*53*, *54*). Hence, the absence of secretion of LOX expressed from constructs lacking the propeptide could be a direct result of the absence of N- and/or O-glycosylation. Another interesting study finds that the presence

of glycosylations assists protein folding co- or posttranslationally and that once folding is achieved, removal of carbohydrate structures do not affect the protein folding and function (*48*). Mature LOX enzyme does not contain N-glycosylation after it is separated from its propeptide (*4*) but is yet catalytically functional. Hence, it is more likely that the glycosylation in the propeptide domain is most important for the biosynthesis, secretion, and targeting of Pro-LOX. A study by Boer et al. (*55*) demonstrated such a requirement for the PGE_2 receptor, EP3-β, where glycosylations were found to be unnecessary for correct protein folding but essential for protein translocation to the plasma membrane.

Proteins, or regions of proteins that are inherently disordered (ID), are recognized as unique entities distinct from fibrous and globular proteins (*56*). ID proteins/regions have amino acid compositions different from ordered proteins (*57*). The amino acid composition and the amino acid sequence of LOX-PP are typical of ID proteins as seen by PONDR analysis software (*39*), suggesting that LOX-PP is largely disordered, confirming previous computer predictions (*15*). Moreover, CD analysis of rLOX-PP revealed a pattern typical of proteins containing random coils, confirming that the predicted disordered structure of LOX-PP is correct.

The recombinant protein produced here has already been used in studies that examine tumor suppressor properties of LOX-PP (*18*, *58*, *59*) and other biological activities of LOX-PP (*19*, *21*). Here we show that the biological activity of LOX-PP is not affected if the protein is preheated to 90 °C, indicating that the propeptide is thermostable, similar to the LOX enzyme (*42*, *43*).

Exogenously added rLOX-PP has been shown to enter cells and associate with microtubules within 2.5 h of exposure, suggesting that LOX-PP could have intracellular functions (*29*). The mechanism of entry of LOX-PP into the cells is at present unknown. It has been proposed that LOX-PP may be able to pass through the lipid bilayer without the aid of a specific cell surface receptor, a property of basic proteins (*14*, *29*). A direct inhibition of purified MEK2 enzyme in vitro by rLOX-PP was recently identified (*19*). The presence of a putative nuclear localization signal (PQRRRDS, residues 39−45) further suggests that intracellular LOX-PP may be actively directed to the nucleus where it was detected (*29*), but its functional activity in the nucleus has not been identified. Other proteins containing inherently disordered structures have been found to have critically important roles in gene regulation, including transcription factors and coactivators (*56*, *60*−*62*). At the same time, rLOX-PP inhibits FGF-2-induced signaling and proliferation of prostate cancer cells via the inhibition of FGF-2 binding to cell surface FGF receptors, supporting an extracellular mechanism for LOX-PP function (*18*). Taken together, findings suggest that LOX-PP could have multiple mechanisms of action. This diversity may be related to its inherently disordered (ID) structure. The inherent flexibility of ID proteins (*57*, *63*, *64*) allows for their local and global structure to be influenced by the structure of binding partners inducing structure and function (*56*, *65*). Hence ID proteins have a large "capture radius" and account for their structural and functional diversity (*60*, *62*, *64*−*66*).

Interestingly, CD analysis of rLOX-PP in the presence of an α-helix inducer, TFE, resulted in acquisition of spectra which indicate the increased presence of α-helical structures. While these spectra are suggestive of a disordered structure, data indicate that LOX-PP is capable of acquiring α-helical content under suitable conditions. Such structural changes could occur in vivo as a consequence of LOX-PP binding to functionally important partners and may contribute to the biological functions of LOX-PP.

ACKNOWLEDGMENT

The authors thank Dr. Olga Gursky, Dr. James C. McKnight, Sunitha Chari, and Dr. Shobini Jayaraman for help with CD spectroscopy and analysis.

SUPPORTING INFORMATION AVAILABLE

Two figures (Figures S1 and S2) containing respectively a Western blot of nondeglycosylated and deglycosylated rLOX-PP and MS3 of an O-glycosylated peptide derived from rLOX-PP. This material is available free of charge via the Internet at http://pubs.acs.org.

REFERENCES

1. Prockop, D. J., and Kivirikko, K. I. (1995) Collagens: molecular biology, diseases, and potentials for therapy. *Annu. Rev. Biochem. 64*, 403–434.
2. Panchenko, M. V., Stetler-Stevenson, W. G., Trubetskoy, O. V., Gacheru, S. N., and Kagan, H. M. (1996) Metalloproteinase activity secreted by fibrogenic cells in the processing of prolysyl oxidase. Potential role of procollagen C-proteinase. *J. Biol. Chem. 271*, 7113–7119.
3. Uzel, M. I., Scott, I. C., Babakhanlou-Chase, H., Palamakumbura, A. H., Pappano, W. N., Hong, H. H., Greenspan, D. S., and Trackman, P. C. (2001) Multiple bone morphogenetic protein 1-related mammalian metalloproteinases process pro-lysyl oxidase at the correct physiological site and control lysyl oxidase activation in mouse embryo fibroblast cultures. *J. Biol. Chem. 276*, 22537–22543.
4. Trackman, P. C., Bedell-Hogan, D., Tang, J., and Kagan, H. M. (1992) Post-translational glycosylation and proteolytic processing of a lysyl oxidase precursor. *J. Biol. Chem. 267*, 8666–8671.
5. Maki, J. M., Tikkanen, H., and Kivirikko, K. I. (2001) Cloning and characterization of a fifth human lysyl oxidase isoenzyme: the third member of the lysyl oxidase-related subfamily with four scavenger receptor cysteine-rich domains. *Matrix Biol. 20*, 493–496.
6. Maki, J. M., and Kivirikko, K. I. (2001) Cloning and characterization of a fourth human lysyl oxidase isoenzyme. *Biochem. J. 355*, 381–387.
7. Kim, Y., Boyd, C. D., and Csiszar, K. (1995) A new gene with sequence and structural similarity to the gene encoding human lysyl oxidase. *J. Biol. Chem. 270*, 7176–7182.
8. Kenyon, K., Modi, W. S., Contente, S., and Friedman, R. M. (1993) A novel human cDNA with a predicted protein similar to lysyl oxidase maps to chromosome 15q24-q25. *J. Biol. Chem. 268*, 18435–18437.
9. Jourdan-Le Saux, C., Tronecker, H., Bogic, L., Bryant-Greenwood, G. D., Boyd, C. D., and Csiszar, K. (1999) The LOXL2 gene encodes a new lysyl oxidase-like protein and is expressed at high levels in reproductive tissues. *J. Biol. Chem. 274*, 12939–12944.
10. Csiszar, K. (2001) Lysyl oxidases: a novel multifunctional amine oxidase family. *Prog. Nucleic Acid Res. Mol. Biol. 70*, 1–32.
11. Mariani, T. J., Trackman, P. C., Kagan, H. M., Eddy, R. L., Shows, T. B., Boyd, C. D., and Deak, S. B. (1992) The complete derived amino acid sequence of human lysyl oxidase and assignment of the gene to chromosome 5 (extensive sequence homology with the murine ras recision gene). *Matrix 12*, 242–248.
12. Contente, S., Kenyon, K., Rimoldi, D., and Friedman, R. M. (1990) Expression of gene rrg is associated with reversion of NIH 3T3 transformed by LTR-c-H-ras. *Science 249*, 796–798.
13. Kenyon, K., Contente, S., Trackman, P. C., Tang, J., Kagan, H. M., and Friedman, R. M. (1991) Lysyl oxidase and rrg messenger RNA. *Science 253*, 802.
14. Palamakumbura, A. H., Jeay, S., Guo, Y., Pischon, N., Sommer, P., Sonenshein, G. E., and Trackman, P. C. (2004) The propeptide domain of lysyl oxidase induces phenotypic reversion of ras-transformed cells. *J. Biol. Chem. 279*, 40593–40600.
15. Min, C., Kirsch, K. H., Zhao, Y., Jeay, S., Palamakumbura, A. H., Trackman, P. C., and Sonenshein, G. E. (2007) The tumor suppressor activity of the lysyl oxidase propeptide reverses the invasive phenotype of Her-2/neu-driven breast cancer. *Cancer Res. 67*, 1105–1112.
16. Wu, M., Min, C., Wang, X., Yu, Z., Kirsch, K. H., Trackman, P. C., and Sonenshein, G. E. (2007) Repression of BCL2 by the tumor

suppressor activity of the lysyl oxidase propeptide inhibits transformed phenotype of lung and pancreatic cancer cells. *Cancer Res. 67*, 6278–6285.
17. Zhao, Y., Min, C., Vora, S., Trackman, P. C., Sonenshein, G. E., and Kirsch, K. H. (2009) The lysyl oxidase pro-peptide attenuates fibronectin-mediated activation of FAK and p130CAS in breast cancer cells. *J. Biol. Chem.* 284, 1385–1393.
18. Palamakumbura, A. H., Vora, S. R., Nugent, M. A., Kirsch, K. H., Sonenshein, G. E., and Trackman, P. C. (2009) Lysyl oxidase propeptide inhibits prostate cancer cell growth by mechanisms that target FGF-2-cell binding and signaling. *Oncogene 28*, 3390–3400.
19. Hurtado, P. A., Vora, S., Sume, S. S., Yang, D., St. Hilaire, C., Guo, Y., Palamakumbura, A. H., Schreiber, B. M., Ravid, K., and Trackman, P. C. (2008) Lysyl oxidase propeptide inhibits smooth muscle cell signaling and proliferation. *Biochem. Biophys. Res. Commun. 366*, 156–161.
20. Hong, H. H., Pischon, N., Santana, R. B., Palamakumbura, A. H., Chase, H. B., Gantz, D., Guo, Y., Uzel, M. I., Ma, D., and Trackman, P. C. (2004) A role for lysyl oxidase regulation in the control of normal collagen deposition in differentiating osteoblast cultures. *J. Cell. Physiol. 200*, 53–62.
21. Vora, S. R., Palamakumbura, A. H., Mitsi, M., Guo, Y., Pischon, N., Nugent, M. A., and Trackman, P. C. (2010) Lysyl oxidase propeptide inhibits FGF-2-induced signaling and proliferation of osteoblasts. *J. Biol. Chem. 285*, 7384–7393.
22. Maki, J. M., Rasanen, J., Tikkanen, H., Sormunen, R., Makikallio, K., Kivirikko, K. I., and Soininen, R. (2002) Inactivation of the lysyl oxidase gene Lox leads to aortic aneurysms, cardiovascular dysfunction, and perinatal death in mice. *Circulation 106*, 2503–2509.
23. Hornstra, I. K., Birge, S., Starcher, B., Bailey, A. J., Mecham, R. P., and Shapiro, S. D. (2003) Lysyl oxidase is required for vascular and diaphragmatic development in mice. *J. Biol. Chem. 278*, 14387–14393.
24. Pischon, N., Maki, J. M., Weisshaupt, P., Heng, N., Palamakumbura, A. H., N'Guessan, P., Ding, A., Radlanski, R., Renz, H., Bronckers, T. A., Myllyharju, J., Kielbassa, A. M., Kleber, B. M., Bernimoulin, J. P., and Trackman, P. C. (2009) Lysyl oxidase (lox) gene deficiency affects osteoblastic phenotype. *Calcif. Tissue Int. 85*, 119–126.
25. Yao, F., Svensjo, T., Winkler, T., Lu, M., Eriksson, C., and Eriksson, E. (1998) Tetracycline repressor, tetR, rather than the tetR-mammalian cell transcription factor fusion derivatives, regulates inducible gene expression in mammalian cells. *Hum. Gene Ther. 9*, 1939–1950.
26. Feres-Filho, E. J., Choi, Y. J., Han, X., Takala, T. E., and Trackman, P. C. (1995) Pre- and post-translational regulation of lysyl oxidase by transforming growth factor-beta 1 in osteoblastic MC3T3-E1 cells. *J. Biol. Chem. 270*, 30797–30803.
27. Eng, J. K., McCormack, A. L., and Yates, J. R. (1994) An approach to correlate tandem mass spectral data of peptides with amino acid sequences in a protein database. *J. Am. Soc. Mass Spectrom. 5*, 976–989.
28. Guo, Y. (2005) Determination of the location and the biological activities of the lysyl oxidase propeptide in osteoblasts. Ph.D. Dissertation, Boston University School of Dental Medicine, Boston, MA.
29. Guo, Y., Pischon, N., Palamakumbura, A. H., and Trackman, P. C. (2007) Intracellular distribution of the lysyl oxidase propeptide in osteoblastic cells. *Am. J. Physiol. Cell. Physiol. 292*, C2095–2102.
30. Scott, I. C., Blitz, I. L., Pappano, W. N., Imamura, Y., Clark, T. G., Steiglitz, B. M., Thomas, C. L., Maas, S. A., Takahara, K., Cho, K. W., and Greenspan, D. S. (1999) Mammalian BMP-1/Tolloid-related metalloproteinases, including novel family member mammalian Tolloid-like 2, have differential enzymatic activities and distributions of expression relevant to patterning and skeletogenesis. *Dev. Biol. 213*, 283–300.
31. Salih, E., and Fluckiger, R. (2004) Complete topographical distribution of both the in vivo and in vitro phosphorylation sites of bone sialoprotein and their biological implications. *J. Biol. Chem. 279*, 19808–19815.
32. Lee, S., Solow-Cordero, D. E., Kessler, E., Takahara, K., and Greenspan, D. S. (1997) Transforming growth factor-beta regulation of bone morphogenetic protein-1/procollagen C-proteinase and related proteins in fibrogenic cells and keratinocytes. *J. Biol. Chem. 272*, 19059–19066.
33. Pisano, A., Packer, N. H., Redmond, J. W., Williams, K. L., and Gooley, A. A. (1994) Characterization of O-linked glycosylation motifs in the glycopeptide domain of bovine kappa-casein. *Glycobiology 4*, 837–844.
34. Schachter, H. (1986) Biosynthetic controls that determine the branching and microheterogeneity of protein-bound oligosaccharides. *Biochem. Cell Biol. 64*, 163–181.
35. Kato, K., Takeuchi, H., Miyahara, N., Kanoh, A., Hassan, H., Clausen, H., and Irimura, T. (2001) Distinct orders of GalNAc incorporation into a peptide with consecutive threonines. *Biochem. Biophys. Res. Commun. 287*, 110–115.
36. Gerken, T. A. (2004) Kinetic modeling confirms the biosynthesis of mucin core 1 (beta-Gal(1−3) alpha-GalNAc-O-Ser/Thr) O-glycan structures are modulated by neighboring glycosylation effects. *Biochemistry 43*, 4137–4142.
37. Julenius, K., Molgaard, A., Gupta, R., and Brunak, S. (2005) Prediction, conservation analysis, and structural characterization of mammalian mucin-type O-glycosylation sites. *Glycobiology 15*, 153–164.
38. Salih, E., Wang, J., Mah, J., and Fluckiger, R. (2002) Natural variation in the extent of phosphorylation of bone phosphoproteins as a function of in vivo new bone formation induced by demineralized bone matrix in soft tissue and bony environments. *Biochem. J. 364*, 465–474.
39. Romero, P., Obradovic, Z., Li, X., Garner, E. C., Brown, C. J., and Dunker, A. K. (2001) Sequence complexity of disordered protein. *Proteins 42*, 38–48.
40. Dunker, A. K., Obradovic, Z., Romero, P., Garner, E. C., and Brown, C. J. (2000) Intrinsic protein disorder in complete genomes. *Genome Inform. Ser. Workshop Genome Inform. 11*, 161–171.
41. Greenfield, N., and Fasman, G. D. (1969) Computed circular dichroism spectra for the evaluation of protein conformation. *Biochemistry 8*, 4108–4116.
42. Jordan, R. E., Milbury, P., Sullivan, K. A., Trackman, P. C., and Kagan, H. M. (1977) Studies on lysyl oxidase of bovine ligamentum nuchae and bovine aorta. *Adv. Exp. Med. Biol. 79*, 531–542.
43. Trackman, P. C., Zoski, C. G., and Kagan, H. M. (1981) Development of a peroxidase-coupled fluorometric assay for lysyl oxidase. *Anal. Biochem. 113*, 336–342.
44. Cronshaw, A. D., Fothergill-Gilmore, L. A., and Hulmes, D. J. (1995) The proteolytic processing site of the precursor of lysyl oxidase. *Biochem. J. 306* (Part 1), 279–284.
45. Vosseller, K., Hansen, K. C., Chalkley, R. J., Trinidad, J. C., Wells, L., Hart, G. W., and Burlingame, A. L. (2005) Quantitative analysis of both protein expression and serine/threonine post-translational modifications through stable isotope labeling with dithiothreitol. *Proteomics 5*, 388–398.
46. Varki, A. (1993) Biological roles of oligosaccharides: all of the theories are correct. *Glycobiology 3*, 97–130.
47. Lis, H., and Sharon, N. (1993) Protein glycosylation. Structural and functional aspects. *Eur. J. Biochem. 218*, 1–27.
48. Shental-Bechor, D., and Levy, Y. (2008) Effect of glycosylation on protein folding: a close look at thermodynamic stabilization. *Proc. Natl. Acad. Sci. U.S.A. 105*, 8256–8261.
49. Dwek, R. A. (1996) Glycobiology: toward understanding the function of sugars. *Chem. Rev. 96*, 683–720.
50. Seve, S., Decitre, M., Gleyzal, C., Farjanel, J., Sergeant, A., Ricard-Blum, S., and Sommer, P. (2002) Expression analysis of recombinant lysyl oxidase (LOX) in myofibroblastlike cells. *Connect. Tissue Res. 43*, 613–619.
51. Kagan, H. M., Reddy, V. B., Panchenko, M. V., Nagan, N., Boak, A. M., Gacheru, S. N., and Thomas, K. M. (1995) Expression of lysyl oxidase from cDNA constructs in mammalian cells: the propeptide region is not essential to the folding and secretion of the functional enzyme. *J. Cell. Biochem. 59*, 329–338.
52. Scheiffele, P., Peranen, J., and Simons, K. (1995) N-glycans as apical sorting signals in epithelial cells. *Nature 378*, 96–98.
53. Ellgaard, L., Molinari, M., and Helenius, A. (1999) Setting the standards: quality control in the secretory pathway. *Science 286*, 1882–1888.
54. Hammond, C., and Helenius, A. (1995) Quality control in the secretory pathway. *Curr. Opin. Cell Biol. 7*, 523–529.
55. Boer, U., Neuschafer-Rube, F., Moller, U., and Puschel, G. P. (2000) Requirement of N-glycosylation of the prostaglandin E2 receptor EP3beta for correct sorting to the plasma membrane but not for correct folding. *Biochem. J. 350* (Part 3), 839–847.
56. Cortese, M. S., Uversky, V. N., and Keith Dunker, A. (2008) Intrinsic disorder in scaffold proteins: getting more from less. *Prog. Biophys. Mol. Biol. 98*, 85–106.
57. Radivojac, P., Iakoucheva, L. M., Oldfield, C. J., Obradovic, Z., Uversky, V. N., and Dunker, A. K. (2007) Intrinsic disorder and functional proteomics. *Biophys. J. 92*, 1439–1456.
58. Min, C., Yu, Z., Kirsch, K. H., Zhao, Y., Vora, S. R., Trackman, P. C., Spicer, D. B., Rosenberg, L., Palmer, J. R., and Sonenshein, G. E. (2009) A loss-of-function polymorphism in the propeptide domain of the LOX gene and breast cancer. *Cancer Res. 69*, 6685–6693.

59. Zhao, Y., Min, C., Vora, S. R., Trackman, P. C., Sonenshein, G. E., and Kirsch, K. H. (2009) The lysyl oxidase pro-peptide attenuates fibronectin-mediated activation of focal adhesion kinase and p130Cas in breast cancer cells. *J. Biol. Chem. 284*, 1385–1393.
60. Wright, P. E., and Dyson, H. J. (1999) Intrinsically unstructured proteins: reassessing the protein structure-function paradigm. *J. Mol. Biol. 293*, 321–331.
61. Iakoucheva, L. M., Brown, C. J., Lawson, J. D., Obradovic, Z., and Dunker, A. K. (2002) Intrinsic disorder in cell-signaling and cancer-associated proteins. *J. Mol. Biol. 323*, 573–584.
62. Dunker, A. K., Brown, C. J., and Obradovic, Z. (2002) Identification and functions of usefully disordered proteins. *Adv. Protein Chem. 62*, 25–49.
63. Fink, A. L. (2005) Natively unfolded proteins. *Curr. Opin. Struct. Biol. 15*, 35–41.
64. Dunker, A. K., Brown, C. J., Lawson, J. D., Iakoucheva, L. M., and Obradovic, Z. (2002) Intrinsic disorder and protein function. *Biochemistry 41*, 6573–6582.
65. Dyson, H. J., and Wright, P. E. (2002) Coupling of folding and binding for unstructured proteins. *Curr. Opin. Struct. Biol. 12*, 54–60.
66. Shoemaker, B. A., Portman, J. J., and Wolynes, P. G. (2000) Speeding molecular recognition by using the folding funnel: the fly-casting mechanism. *Proc. Natl. Acad. Sci. U.S.A. 97*, 8868–8873.